NANO LETTERS

pubs.acs.org/NanoLett Letter

Electron Localization and Mobility in Monolayer Fullerene Networks

Amedeo Capobianco, Julia Wiktor, Alessandro Landi,* Francesco Ambrosio,* and Andrea Peluso

Cite This: *Nano Lett.* 2024, 24, 8335−8342 Read Online

ACCESS | Metrics & More | Article Recommendations | Supporting Information

ABSTRACT: The novel 2D quasi-hexagonal phase of covalently bonded fullerene molecules (qHP C_{60}), the so-called graphullerene, has displayed far superior electron mobilities, if compared to the parent van der Waals three-dimensional crystal (vdW C_{60}). Herein, we present a comparative study of the electronic properties of vdW and qHP C_{60} using state-of-the-art electronic-structure calculations and a full quantum-mechanical treatment of electron transfer. We show that both materials entail polaronic localization of electrons with similar binding energies (≈0.1 eV) and, therefore, they share the same charge transport via polaron hopping. In fact, we quantitatively reproduce the sizable increment of the electron mobility measured for qHP C_{60} and identify its origin in the increased electronic coupling between C_{60} units.

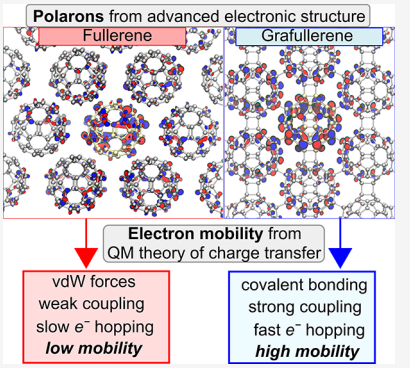

KEYWORDS: *density functional theory calculations, monolayer fullerene networks, polarons in semiconductors, electron mobility*

Synthetic carbon allotropes bearing extended sp^2 hybridization possess unique optoelectronic properties, which mainly derive from quantum confinement.[1,2] For this reason, they have attracted broad interest from the scientific community for a plethora of technological applications, e.g. microelectronics, photovoltaics, and photocatalysis.[3−6]

On the one side, we have buckminsterfullerene, C_{60}, the first synthetic carbon allotrope, which forms a highly stable molecular solid held together by van der Waals (vdW) interactions, cf. Figure 1, indicated in the following as vdW C_{60}.[7,8] Its electronic properties, essentially stemming from those of the isolated molecule, feature narrow bands and a band gap of ∼1.9−2.1 eV,[9,10] suitable for optoelectronics[11−15] and photocatalysis.[16,17] However, together with its morphological instability,[18] the modest electron mobility of vdW C_{60} represents the Achilles heel of the material, as it favors charge recombination and hence limits the final efficiency attainable by the associated devices.[19−21]

On the other side, the pioneering work of Novoselov et al. on graphene[22,23] laid the foundations for the field of two-dimensional (2D) materials, whose peculiar features, deriving from electron confinement in the monolayer limit, can be exploited for a diverse set of applications.[24−29] While acting on the topology of the periodic carbon network has enabled the modulation of the desired electronic properties to a certain extent,[22,23,30] such studies have long been limited to periodic 2D networks whose building blocks are single carbon atoms.

In this context, decades after seminal studies on polymeric C_{60} phases,[31−34] a superatomic equivalent of graphene has been recently synthesized.[35−37] This novel 2D material, named graphullerene,[35] displays C_{60} molecules as vertices of the honeycomb lattice, forming a quasi-hexagonal phase (qHP), cf.

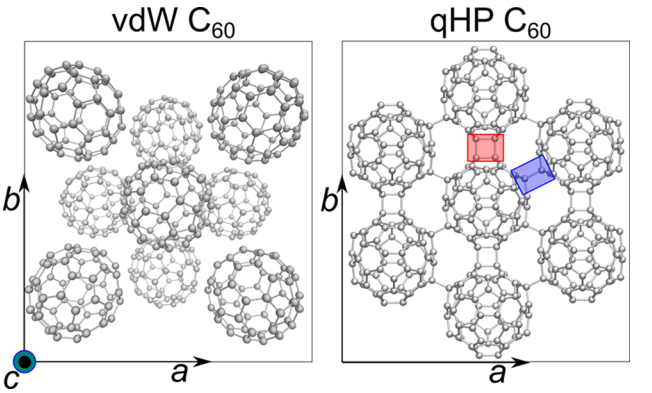

Figure 1. Stick-and-ball representation of the face-centered cubic crystal structure of vdW C_{60} (a shading has been added to emphasize the depth of the cell) and qHP C_{60} in which each unit is covalently bonded with six (nearest) neighbors, four of them connected via a CC single bond and two via collinear [2 + 2] cycloaddition bonds. (blue and red shaded boxes highlight the single and cycloaddition bonds, respectively).

Figure 1. qHP C_{60} is a semiconductor possessing a fundamental band gap of ∼1.6 eV and it exhibits an electron mobility up to 2 orders of magnitude higher than that of vdW

Received: April 10, 2024
Revised: May 10, 2024
Accepted: May 15, 2024
Published: May 20, 2024

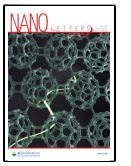

https://doi.org/10.1021/acs.nanolett.4c01695
Nano Lett. 2024, 24, 8335−8342

C_{60}.[35,37] These properties, coupled with stability up to 600 K and good environmental endurance,[37−39] have steadily prompted experimental and theoretical efforts aimed at assessing the feasibility of plentiful technological applications.[40−48]

Unveiling the physics beyond the sizable increase in electron mobility when fullerenes form a covalently bonded network is of undoubted interest for the bottom-up approach in the synthesis of novel materials, based on the use of clusters or "superatoms" as constituents.[49] While it is tempting to address this issue considering band-like transport,[40,45] it should be noted that organic semiconductors, such as vdW C_{60}, may display polaronic localization of charge carriers,[50−55] whose extent, in conjunction with the electronic coupling, is closely linked with the transport mechanism within the material.[56−59]

In particular, for vdW C_{60}, the occurrence of electron polarons has been subject of discussion in the literature. Results based on model Hamiltonians indicated polaronic localization in C_{60}, depending upon π conjugation between molecules.[50] Similar considerations were made in early studies on polymeric chains.[60] More recently, a small barrier for charge transport has been predicted[59] and polaron-mediated transport for qHP C_{60} has been proposed by Cassiano et al.[61] In contrast, a more spread charge carrier is predicted by coarse-grained simulations coupled with a tight-binding model, in which, however, the effect of the added charge is only included indirectly.[62]

In qHP C_{60}, the formation of the 2D polymer comes at the expense of sp^2 hybridization, which is found to be interspersed by sp^3 carbons, forming $C_{60}-C_{60}$ single bonds. These sp^3 carbons are known to hinder electron transfer channels, e.g. in light-harvesting molecules for dye-sensitized solar cells.[63,64] Hence, the enhanced charge mobility of graphullerene may not be a consequence of a change in transport regime but simply stem from shorter interfullerene distances. Overall, within the ongoing debate on the optimal models to predict charge mobility in organic semiconductors and molecular crystals,[56,65,66] graphullerene represents an intriguing model system to gain further understanding of the effects influencing transport mechanisms.

In this Letter, we assess the localization and mobility of extra electrons in qHP C_{60}, by combining advanced electronic-structure calculations with a full quantum mechanical theoretical framework for the calculation of electron transfer rates. Our approach, which is found to excellently reproduce the measured electronic properties of both fullerene and graphullerene, allows us to observe that polaronic localization of electrons, envisaged for the crystalline vdW C_{60} solid, still holds in the covalently bonded network of qHP C_{60}, because of the antibonding nature of its conduction band minimum. Therefore, the transport of both materials can be described by polaron hopping. In fact, the substantial raise in electron mobility measured in experiments for qHP C_{60} with respect to vdW C_{60} is correctly reproduced by our theoretical modeling of charge mobility and it is found to mainly derive from the enhanced electronic coupling between C_{60} units, held together in the honeycomb lattice at closer distances with respect to vdW C_{60}.

We model vdW C_{60} and qHP C_{60} employing supercells, corresponding to the experimental structures at room temperature,[37,69] and including 32 and 16 molecules, respectively (cf. Figure S1). These large supercells are necessary to avoid a charged molecular unit having its periodic replica as a first neighbor. To neutralize the self-interaction error of density functional theory (DFT),[70,71] we employ the Koopmans' compliant class of hybrid functionals[72] based on the PBE0[73,74] family. Nonlocal electron correlation is included in the functional via the rVV10 scheme[75,76] to ensure a correct description of structural properties, cf. Table S2. We refer to the Supporting Information (SI) for details of the calculations and for auxiliary tests of the accuracy of the employed methodology.

We first calculate the fundamental band gap of the two materials at room temperature, $E_g(T)$, combining electronic-structure calculations with molecular dynamics simulations, cf. SI, to account for thermal renormalization, which is often relevant in organic semiconductors (Table S4).[58,77,78] Furthermore, by modeling the relevant semiconductor-vacuum interface (see SI), we also estimate the ionization potential (IP) and electron affinity (EA) of the two carbon allotropes (Table 1). When compared with the 3D crystal, graphullerene

Table 1. Calculated Values of the Electronic Band Gap at Room Temperature $E_g(T)$, the Ionization Potential (IP), and the Electron Affinity (EA) for vdW and qHP C_{60}[a]

Theory	$E_g(T)$	IP	EA
vdW	1.93	6.09	4.16
qHP	1.72	5.86	4.14
Expt.	E_g	IP	EA
vdW	1.9−2.1[9,10]	6.17[67]	3.5 ± 0.9[68]
qHP	1.6[37]		

[a]Experimental estimates, where available, are also reported. All quantities are given in eV.

features an IP = 5.86 eV, shifted by 0.23 eV toward the vacuum level, while the EA (4.14 eV) remains almost unaltered. This suggests that the formation of the honeycomb lattice may have a larger impact on the valence rather then the conduction band edge.

To better understand the correlation between structure and electronic properties, we now focus on qHP C_{60} which is here predicted to be a direct band gap semiconductor at Γ [cf. Figure 2 (a)], in line with a recent study.[45] Its valence and conduction band edges, see Figure 2 (b-c), are akin to those of the parent vdW crystal (cf. Figure S4); However, the electron density of the valence band maximum (VBM) is sizable on both single and cycloaddition of C−C bonds, i.e. it is a bonding orbital; in stark contrast, the conduction band minimum (CBM) displays an antibonding character, with the electron density being confined to the individual C_{60} units, in closer resemblance of vdW C_{60}. Inspection of the electronic density of states, see Figure 2 (d), reveals that both band edges are mainly constituted by p states. When compared to vdW C_{60} (cf. SI), the 2D phase displays a broader and less structured DOS distribution, as the I_h symmetry of the fullerene molecule is here lost. Moreover, the s character of the CBM, while still exiguous is found to be noticeably larger in qHP C_{60}.

We next investigate polaron formation in these materials. First, we calculate the polaron binding energy, defined as

$$\lambda^{\pm}(\mathrm{crys}) = E^{\pm}_{\mathrm{vert}} - E^{\pm}_{\mathrm{opt}} \quad (1)$$

i.e. the difference between the total energy of the relaxed supercell bearing an extra positive or negative charge, $E^{\pm}_{\mathrm{opt}}$, and that of the supercell upon vertical charge injection on the

https://doi.org/10.1021/acs.nanolett.4c01695
Nano Lett. 2024, 24, 8335−8342

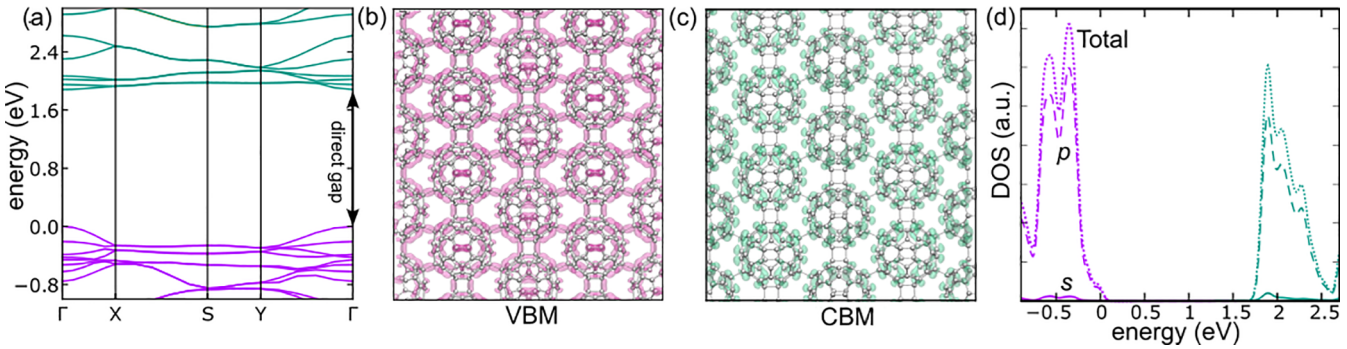

Figure 2. (a) Band structure of qHP C_{60} calculated using the PBE0(α)+rVV10 functional. Valence band are given in purple and conduction bands in teal. Isodensity representation of (b) the valence band maximum and (c) the conduction band minimum. (d) Total and projected electronic density of states of the valence (purple) and conduction band edges (teal) of qHP C_{60}.

neutral system, $E^{\pm}_{vert}$, the latter acting as a reference for the delocalized conduction band edge. In molecular crystals, we can further disentangle the individual contributions to the total binding energy, in analogy with internal and external reorganization energies defined in Marcus theory for electron transfer in solution.[79] In particular, we can define the molecular reorganization energy as[58]

$$\lambda^{\pm}(\mathrm{loc}) = E^{\pm}_{vert} - E^{\pm}_{loc} \quad (2)$$

In eq 2, $E^{\pm}_{loc}$ is the total energy of a charged system in which only a single molecule of the supercell is allowed to relax, while the coordinates of all other atoms are fixed. It follows that the environment response to molecular charge localization is given by

$$\lambda^{\pm}(\mathrm{env}) = \lambda^{\pm}(\mathrm{crys}) - \lambda^{\pm}(\mathrm{loc}) \quad (3)$$

The overall scheme is reported in Figure 3(a) for electron polarons.

The calculated binding energies are reported in Table 2. We here estimate λ^{+}(crys) = 0.18 and λ^{-}(crys) = 0.13 eV for vdW C_{60}, these values originating from relaxation of a single C_{60} molecule, as the external reorganization is found to be negligible, in accordance with the apolar nature of the material. We note that the computed $\lambda^{\pm}$(loc) are in line with those reported in the literature[80−83] for the isolated molecule. At variance with this, no hole localization is predicted for qHP C_{60}, as λ^{+}(crys) is vanishingly small, a result that can be associated with the more dispersive nature of the VBM. As far as the electron is concerned, qHP C_{60} displays a slightly lower value of λ^{-}(crys) = 0.10 eV and different distribution of total binding energy. In fact, λ^{-}(loc) is found to be only 0.07 eV, ca. half of the vdW C_{60} value, a consequence of the more constrained and rigid structure of the C_{60} molecule within the covalently bonded network. However, the contribution to the polaron stabilization induced by the surrounding molecules is more significant, as we calculate λ^{-}(env) = 0.03 eV. In particular, upon relaxation with an extra electron, the single bonds connecting four C_{60} units to that bearing most of the charge are found to be elongated by ≈0.02 Å, while the distances between the centers of mass of the central fullerene molecule and its first neighbors is increased by at most 0.005 Å. This is again in accord with the antibonding nature of the CBM, i.e. weakening of the bond upon addition of an electron. Overall, this weak but collective response partly compensate for the reduced internal reorganization.

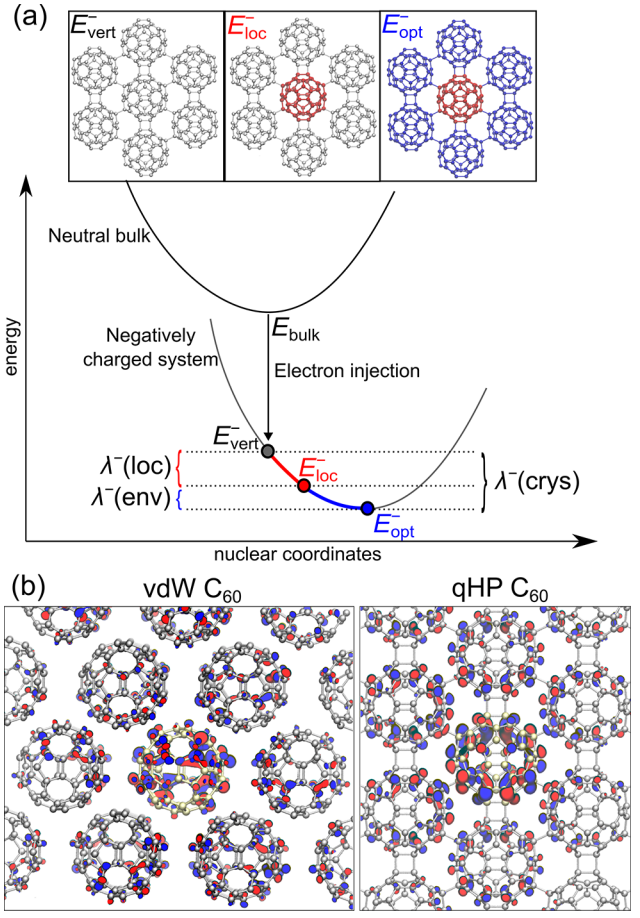

Figure 3. (a) Schematic representation of the calculated binding energies for electron polarons, as defined in the main text. The color code on the structural representation of qHP C_{60} indicates atoms allowed to relax for each calculations: gray (no structural relaxation), red (relaxation of a single molecule) and blue (relaxation of the other molecules). (b) Isodensity representation of the highest occupied molecular orbital (HOMO) for the negatively charged supercells of vdW C_{60} (left panel, side view along the 110 direction) and qHP C_{60} (right panel, top view). C atoms of the molecule featuring most charge localization are given in yellow.

The highest occupied molecular orbitals (HOMO) for the negatively charged supercells, presented in Figure 3 (b), clearly indicate charge localization for both the vdW solid and the 2D monolayer network: for the former, it is primarily distributed on an equatorial ring of a single C_{60},[84] with the electron

https://doi.org/10.1021/acs.nanolett.4c01695
Nano Lett. 2024, 24, 8335−8342

Table 2. Calculated Polaron Binding Energies (cf. Main Text) for vdW and qHP C_{60}[a]

	λ^+(loc)	λ^+(env)	λ^+(crys)
vdW	0.18	<0.01	0.18
qHP			<0.01
	λ^-(loc)	λ^-(env)	λ^-(crys)
vdW	0.13	<0.01	0.13
qHP	0.07	0.03	0.10

[a]All quantities are given in eV.

density slightly extending to the first neighbors; similarly, for the latter, the electron density directed toward the intermolecular bonds. Thus, the observed antibonding character of CBM favors the formation of the electron polaron and the residual delocalization of the charge can be attributed to the same $\pi-\pi$ interactions occurring in vdW C_{60}. The present analysis is confirmed by estimating the inverse participation ratio (IPR), which allows for a quantification of charge confinement. In fact, for both materials, the IPR of the electron polaron is intermediate to those of an isolated C_{60} anion and of the vertically anionized supercell (cf. SI). Such a result is in qualitative agreement with the charge densities recently simulated through model Hamiltonians for qHP C_{60}.[61] Overall, our *ab initio* approach supports polaron formation in vdW C_{60} and unveils that a similar electron localization is preserved in the 2D phase.

We next verify the consistency of this physical picture with the enhanced electron mobility measured for qHP C_{60}, with respect to the vdW crystal. In light of the predicted polaron formation, it is expected that a hopping model should properly describe charge transport in both these materials. Thus, electron hopping rates have been calculated in the framework of Fermi's Golden Rule (FGR), whereby the transition rate between an initial (i) and final (f) state is expressed as

$$k_{ij} = \frac{2\pi}{\hbar}|J_{fi}|^2 F(\Delta E_{fi}, T) \quad (4)$$

In eq 4, J_{fi} is the electronic coupling element, and $F(\Delta E_{fi},T)$ is the Franck–Condon weighted density of states (FCWD), *vide infra*, evaluated at temperature T and at the energy difference ΔE_{fi} between the states.

The electronic coupling J between two neighboring C_{60} units has been evaluated by using the two-state model,[85] by extracting dimers from the crystallographic structures (see SI for details). This static approach in the calculation of J, generally leads to mobilities in fair agreement with the experiment.[86] While all dimers are equivalent in the highly symmetric vdW C_{60} crystal, for qHP C_{60} we need to calculate J for (i) the dimer bound via a single bond (J_s) and (ii) that bearing a cycloaddition bond (J_c), cf. Figure 1 and Table 3. Furthermore, for dimers extracted from qHP C_{60}, hydrogen atoms are added to saturate the valence, where necessary, to have all the sp^3 carbon atoms retaining their character.

For vdW C_{60}, we calculate $|J|$ = 32 meV, a value consistent with those usually assessed for molecular crystals.[87] For qHP C_{60}, we estimate $|J_s|$ = 75 meV and $|J_c|$ = 81 meV, both larger than that of the vdW solid. We also note that the slight difference in the calculated couplings for the two different hopping pathways is in line with the measured preferential conductivity along the [2 + 2] fullerene bonds[37] and can be related with the different chemical bonding.

Table 3. Calculated Electronic Coupling (J, eV), Rates (k, s^{-1}), Diffusion Coefficients (D, cm^2s^{-1}), and Mobility (μ, $cm^2\ V^{-1}\ s^{-1}$) for qHP C_{60} and vdW C_{60}[a]

	path	J	k	D	μ
vdW		0.033	1.3×10^{13}	2.15×10^{-6}	0.84 (0.08–0.3)
qHP	c	0.081	9.28×10^{13}	1.85×10^{-5}	7.20 (5)
	s	0.075	8.15×10^{13}		

[a]Experimental mobilities are given in parentheses.

The difference in coupling between the two materials may be explained in terms of the shorter intermolecular distance between the centers of mass, r_{CM}, within the covalently bonded network (≈ 0.9 Å less than that observed for the fullerene crystal). To substantiate this assumption, we also calculate the coupling between two fullerene molecules at varying r_{CM}: we find J values close to those computed for graphullerene at lower distances, cf. Figure 4 (a). Moreover, when r_{CM} reaches

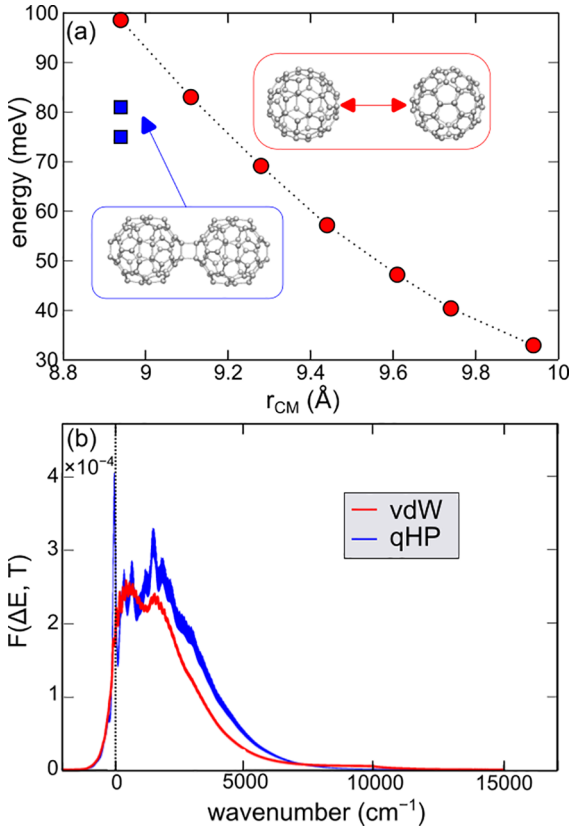

Figure 4. (a) Electronic coupling as a function of the distance between the centers of mass for a nonbonded fullerene dimer (red circles); blue squares indicate the values calculated for covalently bonded dimers (cf. main text). (b)Franck–Condon weighted density of states at T = 298 K as a function of the energy calculated for vdW (red) and qHP (blue) C_{60}. Dotted black line indicates the ΔE value corresponding to the electron transfer reaction.

the same value of the graphullerene 2D network, we calculate J = 100 meV, > 20% higher than both J_s and J_c. This clearly indicates that, while shorter distances enhance the interaction strength, the formation of bonds via sp^3 hybridization and the distortions associated with it weakens the coupling between molecular units, thus further explaining why the electron remains localized also in the covalently bonded lattice.

https://doi.org/10.1021/acs.nanolett.4c01695
Nano Lett. 2024, 24, 8335–8342

Next, we discuss the FCWD appearing in eq 4 which is defined as

$$F(\Delta E_{fi}, T) = \sum_{\mathbf{v}'} \sum_{\mathbf{v}''} w_{\mathbf{v}'}(T) |\langle \mathbf{v}''|\mathbf{v}'\rangle|^2 \delta(E_{i\mathbf{v}'} - E_{f\mathbf{v}''} - \Delta E_{fi}) \quad (5)$$

where $\mathbf{v}'$ and $\mathbf{v}''$denote the vectors of the vibrational quantum states of the $|i\rangle$and $|f\rangle$, respectively, and $w_{\mathbf{v}'}$ are the equilibrium (Boltzmann) population of $|i\rangle\mathbf{v}'$. We here calculate the FCWDs, using the generating function approach (cf. SI and refs.[88−93]) at T = 298 K, considering the optimized isolated molecule for vdW C_{60} and the molecule saturated with hydrogen atoms for qHP C_{60}. From Figure 4, we notice that the FCWD for qHP C_{60} is slightly broader than that of vdW C_{60}, again a consequence of the higher distortion induced by the sp^3 character of the C atoms covalently bonded to other fullerene units in graphullerene. Since we are modeling electron transfer as a polaron hopping between equivalent sites, we focus on the FCWD value at $\Delta E_{fi} = 0$ (cf. SI), which is very similar for vdW and qHP C_{60}. This indicates that the difference in the electron transfer rates (and hence transport properties) for the two systems under study mainly derives from the electronic coupling.

Finally, we determine the drift electron mobility μ according to the Einstein−Smoluchowski's relation:

$$\mu = \frac{eD}{k_B T} \quad (6)$$

where e is the elementary charge, k_B the Boltzmann's constant, and D is the diffusion coefficient here defined as[94]

$$D = \frac{1}{2n} \sum_i r_{CM_i}^2 k_i P_i \quad (7)$$

In eq 7, n is the dimensionality of the system, r_{CM_i} is the distance between the centers of mass of the interacting molecules, k_i is the electron transfer rate, and P_i is the probability of the hop along the i-th pathway given by

$$P_i = \frac{k_i}{\sum_j k_j} \quad (8)$$

For qHP C_{60}, the summation runs over the two charge transfer pathways, accounting for the fact that each fullerene molecule in the honeycomb lattice has four neighbors linked through a single bond and two via a cycloaddition bond. From eq 7, we also note that the shorter interfullerene distances in qHP C_{60} influences D both directly (via r_{CM_i}) and indirectly (i.e., modulating the electronic coupling which determines k_i).

In Table 3, we collect the calculated and measured electron mobilities. For vdW C_{60}, we predict μ = 0.84 $cm^2V^{-1}s^{-1}$, to be confronted with the measured estimates of 0.08−0.3 $cm^2V^{-1}s^{-1}$;[95−97] for qHP C_{60}, we calculate μ = 7.20 $cm^2V^{-1}s^{-1}$, in close agreement with the experimental value of 5 $cm^2V^{-1}s^{-1}$.[35] Overall, our model nicely portrays the increase in mobility when passing from vdW to qHP C_{60} and provides results in very good accord with measurements: The order of magnitude, the only thing one can trust for this delicate quantity, is captured and the slight overestimation for both materials is due to the fact that actual devices contains various impurities,[35−37] which are known to limit mobility.[89,98] The enhancement in electron mobility by almost 1 order of magnitude for qHP C_{60} with respect to the fullerene 3D solid is found to mainly stem from the increase of the electronic coupling, which in turn is mainly related to the shortened distances between neighboring C_{60} units. The covalent bonded network, while serving this purpose, is also found to partially hinder electron transfer, due to the sp^3 carbon atoms impairing intermolecular interactions.

In conclusion, we performed advanced electronic-structure calculations which allowed us to demonstrate that, notwithstanding the different nature of the intermolecular interactions, a similar polaronic localization of electrons is envisaged in vdW and qHP C_{60}, a consequence of the antibonding nature of the CBM of the 2D phase. We then showed that electron hopping within the framework of Fermi's Golden Rule permits to calculate electron mobilities in excellent agreement with the experimental trend and to establish a clear connection between the augmented electronic coupling of neighboring molecules and the enhanced mobility displayed by qHP C_{60}.

■ ASSOCIATED CONTENT

Data Availability Statement

Input files, models, and snapshots of MD simulations are available at https://github.com/fra85uni/graphullerene.

Supporting Information

The Supporting Information is available free of charge at https://pubs.acs.org/doi/10.1021/acs.nanolett.4c01695.

Models of the supercells employed to simulate vdW and qHP C_{60} and computational details of the associated calculations, including details of the probe method employed to define the fraction of Fock exchange α used in the hybrid functional and additional tests on the accuracy of the employed methodology. Computational details of molecular dynamics simulations and calculated band gap and band edges thermal renormalization. Details on the calculation of the FCWD. Additional refs. 99−119 (PDF)

■ AUTHOR INFORMATION

Corresponding Authors

Alessandro Landi − *Dipartimento di Chimica e Biologia Adolfo Zambelli, Università di Salerno, I-84084 Fisciano, Italy;* orcid.org/0000-0003-3627-5535; Email: alelandi1@unisa.it

Francesco Ambrosio − *Dipartimento di Scienze, Università degli Studi della Basilicata, 10-85100 Potenza, Italy; Dipartimento di Chimica e Biologia Adolfo Zambelli, Università di Salerno, I-84084 Fisciano, Italy;* orcid.org/0000-0002-6388-9586; Email: francesco.ambrosio@unibas.it

Authors

Amedeo Capobianco − *Dipartimento di Chimica e Biologia Adolfo Zambelli, Università di Salerno, I-84084 Fisciano, Italy;* orcid.org/0000-0002-5157-9644

Julia Wiktor − *Department of Physics, Chalmers University of Technology, SE-412 96 Gothenburg, Sweden;* orcid.org/0000-0003-3395-1104

Andrea Peluso − *Dipartimento di Chimica e Biologia Adolfo Zambelli, Università di Salerno, I-84084 Fisciano, Italy;* orcid.org/0000-0002-6140-9825

Complete contact information is available at: https://pubs.acs.org/10.1021/acs.nanolett.4c01695

https://doi.org/10.1021/acs.nanolett.4c01695
Nano Lett. 2024, 24, 8335−8342

Notes

The authors declare no competing financial interest.

■ ACKNOWLEDGMENTS

A.L., A.C. and A.P. acknowledge financial support from the Università di Salerno, grants: FARB 2020 and FARB 2021 and they gratefully acknowledge PRIN 2022 grants 2022XSC9P5, P2022WXPMB, and 2022KHEZTC by "Ministero dell'Universit e della Ricerca" (MIUR) for funding. F. A. thankfully acknowledges REACT-EU DM 1062/2021 and PRIN 2022-PNRR grant (P2022W9773) for funding. F.A. also acknowledges the CINECA award under the ISCRA initiative, for the availability of high-performance computing resources (projects AID-Loc and Def-OCS). J.W. acknowledges funding from the Swedish Research Council (2019-03993) and the Swedish Strategic Research Foundation through a Future Research Leader programme (FFL21-0129), and computational resources from the National Academic Infrastructure for Supercomputing in Sweden (NAISS) at C3SE and NSC.

■ REFERENCES

(1) Hirsch, A. The Era of Carbon Allotropes. *Nat. Mater.* **2010**, *9*, 868−871.
(2) Castro Neto, A. H. The Carbon New Age. *Mater. Today* **2010**, *13*, 12−17.
(3) Avouris, P.; Chen, Z.; Perebeinos, V. Carbon-Based Electronics. *Nat. Nanotechnol* **2007**, *2*, 605−615.
(4) Zhu, H.; Wei, J.; Wang, K.; Wu, D. Applications of Carbon Materials in Photovoltaic Solar Cells. *Sol. Energy Mater. Sol. Cells* **2009**, *93*, 1461−1470.
(5) Sahani, S.; Tripathi, K. M.; Lee, T. I.; Dubal, D. P.; Wong, C.-P.; Sharma, Y. C.; Kim, T. Y. Recent Advances in Photocatalytic Carbon-Based Materials for Enhanced Water Splitting under Visible-Light Irradiation. *Energy Convers. Manag.* **2022**, *252*, 115133.
(6) Bramhaiah, K.; Bhattacharyya, S. Challenges and Future Prospects of Graphene-Based Hybrids for Solar Fuel Generation: Moving towards Next Generation Photocatalysts. *Mater. Adv.* **2022**, *3*, 142−172.
(7) Kroto, H. W.; Heath, J. R.; O'Brien, S. C.; Curl, R. F.; Smalley, R. E. C_{60}: Buckminsterfullerene. *Nature* **1985**, *318*, 162−163.
(8) David, W. I.; Ibberson, R. M.; Matthewman, J. C.; Prassides, K.; Dennis, T. J. S.; Hare, J. P.; Kroto, H. W.; Taylor, R.; Walton, D. R. Crystal Structure and Bonding of Ordered C_{60}. *Nature* **1991**, *353*, 147−149.
(9) Rabenau, T.; Simon, A.; Kremer, R.; Sohmen, E. The Energy Gaps of Fullerene C_{60} and C_{70} Determined from the Temperature Dependent Microwave Conductivity. *Z. Phys. B Con. Mater.* **1993**, *90*, 69−72.
(10) Shirley, E. L.; Louie, S. G. Electron Excitations in Solid C_{60}: Energy Gap, Band Dispersions, and Effects of Orientational Disorder. *Phys. Rev. Lett.* **1993**, *71*, 133.
(11) Yu, G.; Gao, J.; Hummelen, J. C.; Wudl, F.; Heeger, A. J. Polymer Photovoltaic cells: Enhanced Efficiencies via a Network of Internal Donor-Acceptor Heterojunctions. *Science* **1995**, *270*, 1789−1791.
(12) Sariciftci, N. S.; Smilowitz, L.; Heeger, A. J.; Wudl, F. Photoinduced Electron Transfer from a Conducting Polymer to Buckminsterfullerene. *Science* **1992**, *258*, 1474−1476.
(13) Collavini, S.; Delgado, J. L. Fullerenes: the Stars of Photovoltaics. *Sustain. Energy Fuels* **2018**, *2*, 2480−2493.
(14) Coro, J.; Suarez, M.; Silva, L. S.; Eguiluz, K. I.; Salazar-Banda, G. R. Fullerene Applications in Fuel Cells: A Review. *Int. J. Hydrog. Energy* **2016**, *41*, 17944−17959.
(15) Landi, A.; Landi, A.; Velardo, A.; Peluso, A. Efficient Charge Dissociation of Triplet Excitons in Bulk Heterojunction Solar Cells. *ACS Appl. Energy Mater.* **2022**, *5*, 10815−10824.
(16) Pan, Y.; Liu, X.; Zhang, W.; Liu, Z.; Zeng, G.; Shao, B.; Liang, Q.; He, Q.; Yuan, X.; Huang, D.; Chen, M. Advances in Photocatalysis Based on Fullerene C_{60} and its Derivatives: Properties, Mechanism, Synthesis, and Applications. *Appl. Catal., B* **2020**, *265*, 118579.
(17) Yao, S.; Yuan, X.; Jiang, L.; Xiong, T.; Zhang, J. Recent Progress on Fullerene-Based Materials: Synthesis, Properties, Modifications, and Photocatalytic Applications. *Materials* **2020**, *13*, 2924.
(18) Lin, Y.; Zhan, X. Non-Fullerene Acceptors for Organic Photovoltaics: an Emerging Horizon. *Mater. Horiz.* **2014**, *1*, 470−488.
(19) Haddon, R.; Perel, A.; Morris, R.; Palstra, T.; Hebard, A.; Fleming, R. C_{60} Thin Film Transistors. *Appl. Phys. Lett.* **1995**, *67*, 121−123.
(20) Frankevich, E.; Maruyama, Y.; Ogata, H. Mobility of Charge Carriers in Vapor-Phase Grown C_{60} Single Crystal. *Chem. Phys. Lett.* **1993**, *214*, 39−44.
(21) Landi, A.; Peluso, A.; Troisi, A. Quantitative Prediction of the Electro-Mechanical Response in Organic Crystals. *Adv. Mater.* **2021**, *33*, 2008049.
(22) Novoselov, K. S.; Geim, A. K.; Morozov, S. V.; Jiang, D.-e.; Zhang, Y.; Dubonos, S. V.; Grigorieva, I. V.; Firsov, A. A. Electric Field Effect in Atomically Thin Carbon Films. *Science* **2004**, *306*, 666−669.
(23) Geim, A. K.; Novoselov, K. S. The Rise of Graphene. *Nat. Mater.* **2007**, *6*, 183−191.
(24) Novoselov, K. S.; Fal' ko, V. I.; Colombo, L.; Gellert, P. R.; Schwab, M. G.; Kim, K. A Roadmap for Graphene. *Nature* **2012**, *490*, 192−200.
(25) Wang, Q. H.; Kalantar-Zadeh, K.; Kis, A.; Coleman, J. N.; Strano, M. S. Electronics and Optoelectronics of Two-Dimensional Transition Metal Dichalcogenides. *Nat. Nanotechnol.* **2012**, *7*, 699−712.
(26) Li, L.; Yu, Y.; Ye, G. J.; Ge, Q.; Ou, X.; Wu, H.; Feng, D.; Chen, X. H.; Zhang, Y. Black Phosphorus Field-Effect Transistors. *Nat. Nanotechnol.* **2014**, *9*, 372−377.
(27) Li, X.; Yu, J.; Wageh, S.; Al-Ghamdi, A. A.; Xie, J. Graphene in Photocatalysis: A Review. *Small* **2016**, *12*, 6640−6696.
(28) Mounet, N.; Gibertini, M.; Schwaller, P.; Campi, D.; Merkys, A.; Marrazzo, A.; Sohier, T.; Castelli, I. E.; Cepellotti, A.; Pizzi, G.; et al. Two-Dimensional Materials from High-Throughput Computational Exfoliation of Experimentally Known Compounds. *Nat. Nanotechnol.* **2018**, *13*, 246−252.
(29) Ares, P.; Novoselov, K. S. Recent Advances in Graphene and Other 2D Materials. *Nano Mater. Sci.* **2022**, *4*, 3−9.
(30) Yu, H.; Xue, Y.; Li, Y. Graphdiyne and its Assembly Architectures: Synthesis, Functionalization, and Applications. *Adv. Mater.* **2019**, *31*, 1803101.
(31) Rao, A.; Zhou, P.; Wang, K.-A.; Hager, G.; Holden, J.; Wang, Y.; Lee, W.-T.; Bi, X.-X.; Eklund, P.; Cornett, D.; et al. Photoinduced Polymerization of Solid C_{60} Films. *Science* **1993**, *259*, 955−957.
(32) Okada, S.; Saito, S. Electronic Structure and Energetics of Pressure-Induced Two-Dimensional C_{60} polymers. *Phys. Rev. B* **1999**, *59*, 1930−1936.
(33) Blank, V. D.; Buga, S. G.; Dubitsky, G. A.; Serebryanaya, N. R.; Popov, M. Y.; Sundqvist, B. High-Pressure Polymerized Phases of C_{60}. *Carbon* **1998**, *36*, 319−343.
(34) Yamanaka, S.; Kubo, A.; Inumaru, K.; Komaguchi, K.; Kini, N.; Inoue, T.; Irifune, T. Electron Conductive Three-Dimensional Polymer of Cuboidal C_{60}. *Phys. Rev. Lett.* **2006**, *96*, 076602.
(35) Meirzadeh, E.; Evans, A. M.; Rezaee, M.; Milich, M.; Dionne, C. J.; Darlington, T. P.; Bao, S. T.; Bartholomew, A. K.; Handa, T.; Rizzo, D. J.; et al. A Few-Layer Covalent Network of Fullerenes. *Nature* **2023**, *613*, 71−76.
(36) Gottfried, J. M. Molecular Soccer Balls Connected to Make a 2D Material. *Nature* **2022**, *606*, 470−471.
(37) Hou, L.; Cui, X.; Guan, B.; Wang, S.; Li, R.; Liu, Y.; Zhu, D.; Zheng, J. Synthesis of a Monolayer Fullerene Network. *Nature* **2022**, *606*, 507−510.

https://doi.org/10.1021/acs.nanolett.4c01695
Nano Lett. 2024, 24, 8335−8342

(38) Peng, B. Stability and Strength of Monolayer Polymeric C_{60}. *Nano Lett.* **2023**, *23*, 652−658.
(39) Shen, G.; Li, L.; Tang, S.; Jin, J.; Chen, X.-J.; Peng, Q. Stability and Elasticity of Quasi-Hexagonal Fullerene Monolayer from First-Principles Study. *Crystals* **2023**, *13*, 224.
(40) Yu, L.; Xu, J.; Peng, B.; Qin, G.; Su, G. Anisotropic Optical, Mechanical, and Thermoelectric Properties of Two-Dimensional Fullerene Networks. *J. Phys. Chem. Lett.* **2022**, *13*, 11622−11629.
(41) Tromer, R. M.; Ribeiro, L. A., Jr.; Galvão, D. S. A DFT study of the Electronic, Optical, and Mechanical Properties of a Recently Synthesized Monolayer Fullerene Network. *Chem. Phys. Lett.* **2022**, *804*, 139925.
(42) Dong, H.; Cao, C.; Ying, P.; Fan, Z.; Qian, P.; Su, Y. Anisotropic and High Thermal Conductivity in Monolayer Quasi-Hexagonal Fullerene: A Comparative Study Against Bulk Phase Fullerene. *Int. J. Heat Mass Transfer* **2023**, *206*, 123943.
(43) Li, W.; Yang, R.; Sun, M. Superior Thermoelectric Properties of Bulk and Monolayer Fullerene Networks. *J. Mater. Chem. A* **2023**, *11*, 3949−3960.
(44) Mortazavi, B. Structural, Electronic, Thermal and Mechanical Properties of C_{60}-Based Fullerene Two-Dimensional Networks Explored by First-Principles and Machine Learning. *Carbon* **2023**, *213*, 118293.
(45) Peng, B. Monolayer Fullerene Networks as Photocatalysts for Overall Water Splitting. *J. Am. Chem. Soc.* **2022**, *144*, 19921−19931.
(46) Wang, T.; Zhang, L.; Wu, J.; Chen, M.; Yang, S.; Lu, Y.; Du, P. Few-Layer Fullerene Network for Photocatalytic Pure Water Splitting into H_2 and H_2O_2. *Angew. Chem., Int. Ed.* **2023**, *135*, e202311352.
(47) Tong, Y.; Liu, H.; Dai, S.; Jiang, D.-e. Jiang, D.-e. Monolayer Fullerene Membranes for Hydrogen Separation. *Nano Lett.* **2023**, *23*, 7470−7476.
(48) Chang, X.; Liu, X.; Zheng, W.; Zhou, L.; Zhang, J. Monolayer Fullerene Network: A Promising Material for VOCs Sensor. *Appl. Surf. Sci.* **2023**, *637*, 157909.
(49) Jena, P.; Sun, Q. Super Atomic Clusters: Design Rules and Potential for Building Blocks of Materials. *Chem. Rev.* **2018**, *118*, 5755−5870.
(50) Belosludov, V. R.; Inerbaev, T. M.; Belosludov, R. V.; Kawazoe, Y. Polaron in a One-Dimensional C_{60} crystal. *Phys. Rev. B* **2003**, *67*, 155410.
(51) Rice, B.; Guilbert, A. A.; Frost, J. M.; Nelson, J. Polaron States in Fullerene Adducts Modeled by Coarse-Grained Molecular Dynamics and Tight Binding. *J. Phys. Chem. Lett.* **2018**, *9*, 6616−6623.
(52) d'Avino, G.; Olivier, Y.; Muccioli, L.; Beljonne, D. Do Charges Delocalize over Multiple Molecules in Fullerene Derivatives? *J. Mater. Chem. C* **2016**, *4*, 3747−3756.
(53) Pereira, M. L., Jr; da Cunha, W. F.; de Sousa, R. T., Jr; e Silva, G. M.; Ribeiro, L. A., Jr Stationary and Dynamical Properties of Polarons in Anisotropic C_{60}-Crystals. *J. Phys. Chem. C* **2019**, *123*, 13410−13418.
(54) Volpi, R.; Kottravel, S.; Nørby, M. S.; Stafstrom, S.; Linares, M. Effect of Polarization on the Mobility of C_{60}: A Kinetic Monte Carlo Study. *J. Chem. Theory Comput.* **2016**, *12*, 812−824.
(55) Richler, K.-D.; Mayou, D. Influence of Static Disorder and Polaronic Band Formation on the Interfacial Electron Transfer in Organic Photovoltaic Devices. *Phys. Rev. B* **2019**, *99*, 195151.
(56) Fratini, S.; Mayou, D.; Ciuchi, S. The Transient Localization Scenario for Charge Transport in Crystalline Organic Materials. *Adv. Funct. Mater.* **2016**, *26*, 2292−2315.
(57) Ciuchi, S.; Hatch, R. C.; Höchst, H.; Faber, C.; Blase, X.; Fratini, S. Molecular Fingerprints in the Electronic Properties of Crystalline Organic Semiconductors: From Experiment to Theory. *Phys. Rev. Lett.* **2012**, *108*, 256401.
(58) Ambrosio, F.; Wiktor, J.; Landi, A.; Peluso, A. Charge Localization in Acene Crystals from Ab Initio Electronic Structure. *J. Phys. Chem. Lett.* **2023**, *14*, 3343−3351.
(59) Yang, H.; Gajdos, F.; Blumberger, J. Intermolecular Charge Transfer Parameters, Electron-Phonon Couplings, and the Validity of Polaron Hopping Models in Organic Semiconducting Crystals: Rubrene, Pentacene, and C_{60}. *J. Phys. Chem. C* **2017**, *121*, 7689−7696.
(60) Springborg, M. Structural and Electronic Properties of Polymeric Fullerene Chains. *Phys. Rev. B* **1995**, *52*, 2935−2940.
(61) Cassiano, T. S. A.; Pereira, M. L.; e Silva, G. M.; de Oliveira Neto, P. H.; Ribeiro, L. A. Large Polarons in Two-Dimensional Fullerene Networks: The Crucial Role of Anisotropy in Charge Transport. *Nanoscale* **2024**, *16*, 2337−2346.
(62) Oberhofer, H.; Reuter, K.; Blumberger, J. Charge Transport in Molecular Materials: An Assessment of Computational Methods. *Chem. Rev.* **2017**, *117*, 10319−10357.
(63) Martsinovich, N.; Troisi, A. High-Throughput Computational Screening of Chromophores for Dye-Sensitized Solar Cells. *J. Phys. Chem. C* **2011**, *115*, 11781−11792.
(64) Ambrosio, F.; Martsinovich, N.; Troisi, A. Effect of the anchoring group on electron injection: theoretical study of phosphonated dyes for dye-sensitized solar cells. *J. Phys. Chem. C* **2012**, *116*, 2622−2629.
(65) Fratini, S.; Ciuchi, S.; Mayou, D.; De Laissardière, G. T.; Troisi, A. A Map of High-Mobility Molecular Semiconductors. *Nat. Mater.* **2017**, *16*, 998−1002.
(66) Kirchartz, T.; Nelson, J. *Topics in Current Chemistry*; Springer: Berlin Heidelberg, 2013; pp 279−324.
(67) Sato, N.; Saito, Y.; Shinohara, H. Threshold ionization energy of C60 in the solid state. *Chem. Phys.* **1992**, *162*, 433−438.
(68) Schwenn, P. E.; Burn, P. L.; Powell, B. J. Calculation of solid state molecular ionisation energies and electron affinities for organic semiconductors. *Org. Electron.* **2011**, *12*, 394−403.
(69) Dorset, D. L.; McCourt, M. P. Disorder and the Molecular Packing of C_{60} Buckminsterfullerene: A Direct Electron-Crystallographic Analysis. *Acta Crystallogr. A* **1994**, *50*, 344−351.
(70) Perdew, J. P.; Zunger, A. Self-Interaction Correction to Density-Functional Approximations for Many-Electron Systems. *Phys. Rev. B* **1981**, *23*, 5048−5079.
(71) Zhang, Y.; Yang, W. A Challenge for Density Functionals: Self-Interaction Error Increases for Systems with a Noninteger Number of Electrons. *J. Chem. Phys.* **1998**, *109*, 2604−2608.
(72) Miceli, G.; Chen, W.; Reshetnyak, I.; Pasquarello, A. Nonempirical Hybrid Functionals for Band Gaps and Polaronic Distortions in Solids. *Phys. Rev. B* **2018**, *97*, 121112.
(73) Perdew, J. P.; Ernzerhof, M.; Burke, K. Rationale for Mixing Exact Exchange with Density Functional Approximations. *J. Chem. Phys.* **1996**, *105*, 9982−9985.
(74) Adamo, C.; Barone, V. Toward Reliable Density Functional Methods without Adjustable Parameters: The PBE0Model. *J. Chem. Phys.* **1999**, *110*, 6158−6170.
(75) Vydrov, O. A.; Van Voorhis, T. Nonlocal van der Waals Density Functional: The Simpler the Better. *J. Chem. Phys.* **2010**, *133*, 244103.
(76) Sabatini, R.; Gorni, T.; de Gironcoli, S. Nonlocal van der Waals Density Functional Made Simple and Efficient. *Phys. Rev. B* **2013**, *87*, 041108.
(77) Brown-Altvater, F.; Antonius, G.; Rangel, T.; Giantomassi, M.; Draxl, C.; Gonze, X.; Louie, S. G.; Neaton, J. B. Band Gap Renormalization, Carrier Mobilities, and the Electron-Phonon Self-Energy in Crystalline Naphthalene. *Phys. Rev. B* **2020**, *101*, 165102.
(78) Rangel, T.; Berland, K.; Sharifzadeh, S.; Brown-Altvater, F.; Lee, K.; Hyldgaard, P.; Kronik, L.; Neaton, J. B. Structural and Excited-State Properties of Oligoacene Crystals from First Principles. *Phys. Rev. B* **2016**, *93*, 115206.
(79) Barbara, P. F.; Meyer, T. J.; Ratner, M. A. Contemporary Issues in Electron Transfer Research. *J. Phys. Chem.* **1996**, *100*, 13148−13168.
(80) Kwiatkowski, J. J.; Frost, J. M.; Nelson, J. The effect of Morphology on Electron Field-Effect Mobility in Disordered C_{60} Thin Films. *Nano Lett.* **2009**, *9*, 1085−1090.
(81) Ide, J.; Fazzi, D.; Casalegno, M.; Meille, S. V.; Raos, G. Electron Transport in Crystalline PCBM-like Fullerene Derivatives: a Comparative Computational Study. *J. Mater. Chem. C* **2014**, *2*, 7313−7325.

https://doi.org/10.1021/acs.nanolett.4c01695
Nano Lett. 2024, 24, 8335−8342

(82) Oberhofer, H.; Blumberger, J. Revisiting Electronic Couplings and Incoherent Hopping Models for Electron Transport in Crystalline C_{60} at Ambient Temperatures. *Phys. Chem. Chem. Phys.* **2012**, *14*, 13846−13852.
(83) Cho, E.; Coropceanu, V.; Brédas, J.-L. Hole versus electron transport in fullerenes. *Org. Electron.* **2023**, *118*, 106798.
(84) Friedman, B. Polarons in C_{60}. *Phys. Rev. B* **1992**, *45*, 1454−1457.
(85) Manna, D.; Blumberger, J.; Martin, J. M. L.; Kronik, L. Prediction of Electronic Couplings for Molecular Charge Transfer Using Optimally Tuned Range-Separated Hybrid Functionals. *Mol. Phys.* **2018**, *116*, 2497−2505.
(86) Nematiaram, T.; Troisi, A. Modeling Charge Transport in High-Mobility Molecular Semiconductors: Balancing Electronic Structure and Quantum Dynamics Methods with the Help of Experiments. *J. Chem. Phys.* **2020**, *152*, 190902.
(87) Landi, A.; Troisi, A. Rapid Evaluation of Dynamic Electronic Disorder in Molecular Semiconductors. *J. Phys. Chem. C* **2018**, *122*, 18336−18345.
(88) Kubo, R.; Toyozawa, Y. Application of the Method of Generating Function to Radiative and Non-Radiative Transitions of a Trapped Electron in a Crystal. *Prog. Theor. Phys.* **1955**, *13*, 160−182.
(89) Landi, A. Charge Mobility Prediction in Organic Semiconductors: Comparison of Second-Order Cumulant Approximation and Transient Localization Theory. *J. Phys. Chem. C* **2019**, *123*, 18804−18812.
(90) Capobianco, A.; Landi, A.; Peluso, A. Modeling DNA Oxidation in Water. *Phys. Chem. Chem. Phys.* **2017**, *19*, 13571−13578.
(91) Velardo, A.; Borrelli, R.; Capobianco, A.; Landi, A.; Peluso, A. Disentangling Electronic and Vibrational Effects in the Prediction of Band Shapes for Singlet-Triplet Transitions. *J. Phys. Chem. C* **2019**, *123*, 14173−14179.
(92) Landi, A.; Capobianco, A.; Peluso, A. Coherent Effects in Charge Transport in Molecular Wires: Toward a Unifying Picture of Long-Range Hole Transfer in DNA. *J. Phys. Chem. Lett.* **2020**, *11*, 7769−7775.
(93) Borrelli, R.; Peluso, A. Elementary Electron Transfer Reactions: From Basic Concepts to Recent Computational Advances. *WIREs: Comput. Mol. Sci.* **2013**, *3*, 542−559.
(94) Wang, L.; Nan, G.; Yang, X.; Peng, Q.; Li, Q.; Shuai, Z. Computational Methods for Design of Organic Materials with High Charge Mobility. *Chem. Soc. Rev.* **2010**, *39*, 423−434.
(95) Kobayashi, S.; Takenobu, T.; Mori, S.; Fujiwara, A.; Iwasa, Y. C_{60} Thin-Film Transistors with High Field-Effect Mobility, Fabricated by Molecular Beam Deposition. *Sci. Technol. Adv. Mater.* **2003**, *4*, 371−375.
(96) Haddon, R. C. C. C_{70} Thin Film Transistors. *J. Am. Chem. Soc.* **1996**, *118*, 3041−3042.
(97) Kobayashi, S.; Takenobu, T.; Mori, S.; Fujiwara, A.; Iwasa, Y. Fabrication and Characterization of C_{60} Thin-Film Transistors with High Field-Effect Mobility. *Appl. Phys. Lett.* **2003**, *82*, 4581−4583.
(98) Fratini, S.; Ciuchi, S.; Mayou, D.; De Laissardière, G. T.; Troisi, A. A Map of High-Mobility Molecular Semiconductors. *Nat. Mater.* **2017**, *16*, 998−1002.
(99) Hartwigsen, C.; Goedecker, S.; Hutter, J. Relativistic Separable Dual-Space Gaussian Pseudopotentials from H to Rn. *Phys. Rev. B* **1998**, *58*, 3641−3662.
(100) Freysoldt, C.; Neugebauer, J.; Van de Walle, C. G. Fully *Ab Initio* Finite-Size Corrections for Charged-Defect Supercell Calculations. *Phys. Rev. Lett.* **2009**, *102*, 016402.
(101) Chen, W.; Pasquarello, A. Correspondence of Defect Energy Levels in Hybrid Density Functional Theory and Many-Body Perturbation Theory. *Phys. Rev. B* **2013**, *88*, 115104.
(102) Komsa, H.-P.; Rantala, T. T.; Pasquarello, A. Finite-Size Supercell Correction Schemes for Charged Defect Calculations. *Phys. Rev. B* **2012**, *86*, 045112.
(103) Eklund, P.; Rao, A.; Wang, Y.; Zhou, P.; Wang, K.-A.; Holden, J.; Dresselhaus, M.; Dresselhaus, G. Optical properties of C_{60}- and C_{70}-Based Solid Films. *Thin solid films* **1995**, *257*, 211−232.
(104) Ren, S.; Wang, Y.; Rao, A.; McRae, E.; Holden, J.; Hager, T.; Wang, K.; Lee, W.-T.; Ni, H.; Selegue, J.; et al. Ellipsometric Determination of the Optical Constants of C_{60} (Buckminsterfullerene) films. *Appl. Phys. Lett.* **1991**, *59*, 2678−2680.
(105) Perdew, J. P.; Burke, K.; Ernzerhof, M. Generalized Gradient Approximation Made Simple. *Phys. Rev. Lett.* **1996**, *77*, 3865.
(106) Umari, P.; Pasquarello, A. Ab initio Molecular Dynamics in a Finite Homogeneous Electric Field. *Phys. Rev. Lett.* **2002**, *89*, 157602.
(107) Ambrosio, F.; Miceli, G.; Pasquarello, A. Structrural, Dynamical and Electronic Properties of Liquid Water: A Hybrid Functional Study. *J. Chem. Phys. B* **2016**, *120*, 7456−7470.
(108) Boys, S. F.; Bernardi, F. The Calculation of Small Molecular Interactions by the Differences of Separate Total Energies. Some Procedures with Reduced Errors. *Mol. Phys.* **1970**, *19*, 553−566.
(109) Cutini, M.; Civalleri, B.; Corno, M.; Orlando, R.; Brandenburg, J. G.; Maschio, L.; Ugliengo, P. Assessment of Different Quantum Mechanical Methods for the Prediction of Structure and Cohesive Energy of Molecular Crystals. *J. Chem. Theory Comput.* **2016**, *12*, 3340−3352.
(110) Martínez-Herrera, M.; Campos, M.; Torres, L. A.; Rojas, A. Enthalpies of Sublimation of Fullerenes by Thermogravimetry. *Thermochim. Acta* **2015**, *622*, 72−81.
(111) Berland, K.; Hyldgaard, P. Exchange Functional That Tests the Robustness of the Plasmon Description of the Van Der Waals Density Functional. *Phys. Rev. B* **2014**, *89*, 035412.
(112) Borrelli, R.; Di Donato, M.; Peluso, A. Role of Intramolecular Vibrations in Long-range Electron Transfer between Pheophytin and Ubiquinone in Bacterial Photosynthetic Reaction Centers. *Biophys. J.* **2005**, *89*, 830−841.
(113) Borrelli, R.; Peluso, A. *MolFC: A Program for Franck-Condon Integrals Calculation*. https://github.com/rborrelli/molfc, accessed January 2024.
(114) Kresse, G.; Hafner, J. Ab Initio Molecular Dynamics for Liquid Metals. *Phys. Rev. B* **1993**, *47*, 558.
(115) Kresse, G.; Furthmüller, J. Efficient Iterative Schemes for Ab Initio Total-Energy Calculations Using a Plane-Wave Basis Set. *Phys. Rev. B* **1996**, *54*, 11169.
(116) VandeVondele, J.; Krack, M.; Mohamed, F.; Parrinello, M.; Chassaing, T.; Hutter, J. Quickstep: Fast and Accurate Density Functional Calculations Using a Mixed Gaussian and Plane Waves Approach. *Comput. Phys. Commun.* **2005**, *167*, 103−128.
(117) Guidon, M.; Schiffmann, F.; Hutter, J.; VandeVondele, J. Ab Initio Molecular Dynamics Using Hybrid Density Functionals. *J. Chem. Phys.* **2008**, *128*, 214104.
(118) Guidon, M.; Hutter, J.; VandeVondele, J. Robust Periodic Hartree-Fock Exchange for Large-Scale Simulations Using Gaussian Basis Sets. *J. Chem. Theory Comput.* **2009**, *5*, 3010−3021.
(119) Guidon, M.; Hutter, J.; VandeVondele, J. Auxiliary Density Matrix Methods for Hartree-Fock Exchange Calculations. *J. Chem. Theory Comput.* **2010**, *6*, 2348−2364.

https://doi.org/10.1021/acs.nanolett.4c01695
Nano Lett. 2024, 24, 8335−8342